Assessing the performance of a plastic optical fiber turbidity sensor for measuring post-fire erosion from plot to catchment scale

J.J. Keizer[1*], M.A.S. Martins[1], S.A. Prats[1], L.F. Santos[1], D.C.S. Vieira[1], R. Nogueira[2], L. Bilro[2]

1. Earth surface processes team, Centre for Environmental and Marine Studies (CESAM), Dept. Environment and Planning, University of Aveiro, Campus Universitário de Santiago, 3810-193 Aveiro, Portugal

2. Institute for Telecommunications, Aveiro (IT-Aveiro), Campus Universitário de Santiago, 3810-193 Aveiro, Portugal

* corresponding author: jjkeizer@ua.pt

Abstract

This study is the first comprehensive testing of a novel plastic optical fiber turbidity sensor with runoff samples collected in the field and, more specifically, with a total of 158 streamflow samples and 925 overland flow samples from a recently burnt forest area in north-central Portugal, collected mainly during the first year after the wildfire, as well as with 56 overland flow samples from a nearby long-unburnt study site. Sediment concentrations differed less between overland flow and streamflow samples than between study sites and, at one study site, between plots with and without effective erosion mitigation treatments. Maximum concentrations ranged from 0.91 to 8.19 gL-1 for the

micro-plot overland flow samples from the six burnt sites, from 1.74 to 8.99 gL-1 for the slope-scale overland flow samples from these same sites, and amounted to 4.55 gL-1 for the streamflow samples. Power functions provided (reasonably) good fits to the - expected - relationships of increasing normalized light loss with increasing sediment concentrations for the different sample types from individual study sites. The corresponding adjusted R^2's that ranged from 0.64 to 0.81 in the case of the micro-plot samples from the six burnt sites, from 0.72 to o.89 in the case of the slope-scale samples from these same sites, and was 0.85 in the case of the streamflow samples. While the overall performance of the sensor was thus rather satisfactory, the results pointed to the need for scale- of site-specific calibrations to maximize reliability of the predictions of sediment concentration by the POF sensor. This especially applied to the cases in which sediment concentration were comparatively low, for example following mulching with forest residues.

1. Introduction

Wildfires are now widely recognized as a potential driver of conspicuous changes in geo-morphological and hydrological processes, through their direct effects on vegetation, litter layer and topsoil (Shakesby, 2011; Moody et al., 2013). Studies across the globe have shown strong and sometimes extreme responses in runoff and erosion in recently burnt areas, especially during the earlier stages of the so-called window-of-disturbance (e.g. Cerdà, 1998; Lane et al., 2006; Robichaud et al., 2007). Nonetheless, important research gaps remain with respect to wildfire impacts on runoff and especially soil erosion, in part due to the relatively limited number of post-fire erosion studies as compared to erosion studies in agricultural areas (Shakesby, 2011). The latter is well-illustrated by the four studies that appear to have been carried out in the Mediterranean Basin on sediment yields from recently burnt catchments (Lavabre and Martin, 1997; Inbar et al., 1998; Mayor et al., 2007; Keizer et al., 2015). Clearly more studies have been published on post-fire erosion at the plot-to-slope scale in the Mediterranean Basin (e.g. Thomas et al., 1999; Fernández et al., 2007; Prats et al., 2014). However, they have typically addressed soil losses with a relatively coarse temporal resolution, i.e. multiple runoff events, which is hampering further insight in underlying sediment transport processes.

The advantages of employing turbidity sensors in erosion studies has been increasingly recognized since their introduction more than two decades ago (Downing, 2006). Nonetheless, commercially-available turbidity sensors such as the "OBS-3+ Suspended Solids and Turbidity Monitor" (©Campbell) typically require complex installations, extensive calibration to local conditions, and, perhaps most importantly, considerable financial resources for their purchase. Fiber optical turbidity sensors and, in particular, those using plastic optical fibers (POF) are now widely viewed to offer various important advantages over traditional methods of sensing (Zienmann, 2008). POF sensors are not only comparatively inexpensive but also easy to handle, immune to electromagnetic interferences, and can easily be used in multi-sensor schemes (Yeo, 2008). This would, amongst others, allow to obtain continuous in-situ recording of sediment concentrations in plot-scale studies and to reduce substantially laboratory efforts by substituting standard methods for at least a large part of the runoff samples.

Various authors (Ruhl et al., 2001; Campbell et al., 2005; Postolache et al., 2007) have obtained promising results with POF sensors to measure turbidity of aqueous solutions over the past decade. Nonetheless, in their review study, Omar and MatJafri (2009) identified the need for more extensive testing, in particular also with respect to dependence on particle size. Therefore, this study aimed to further test the performance of the POF sensor developed by Bilro et al. (2010), which had provided promising results for contrasting suspended materials, including ashes from recently burnt areas (Bilro et al., 2011). More specifically, this study wanted to: (i) assess the performance of this sensor for measuring sediment concentration of post-fire runoff generated during the initial stages of the “window-of-disturbance”, when erosion rates are expectedly highest; (ii) evaluate if sensor performance differed for stream flow and for overland flow from erosion plots with contrasting runoff areas (micro-plots vs. slope-scale plots) and, thus, potentially different erosion processes (inter-rill erosion vs. rill/gully erosion); (iii) determine if sensor performance depended on land cover, parent material and site-specific conditions. This study was envisaged as an important step towards the development of a commercial version of the sensor designed by Bilro et al. (2010).

2. Study area and sites

This study was carried out near the hamlet of Ermida in the Sever do Vouga municipality of north-central Portugal (Figure 1). The area was burnt by a wildfire that took place between the 26th and 28th of July 2010 and that affected some 300 ha (DUDF, 2011). By the time of the fire, the area was mainly covered by plantations of eucalypt (Eucalyptus globulus Labill.)

but did include some plantations of maritime pine (Pinus pinaster Ait.). The severity of the wildfire (sensu Keely, 2009) was assessed in the field using as indicators ash colour as well as degree of tree crown scorching and of litter layer consumption, following Shakesby and Doerr (2006) and prior studies in the region such as Malvar et al. (2011, 2013). At all six study sites selected within the burnt area (Figure 1), fire severity was classified as moderate. During the winter of 2010/11, the central part of the study area was bench terraced using a bull dozer, affecting three of the study sites (the terraces are clearly visible in Figure 1).

The climate of the study area can be classified as humid meso-thermal (Csb, according to the Köppen classification), with moderately dry but extended summers (DRA-Centro, 1998). The parent material in the study area mainly consisted of pre-Ordovician schists but included Hercynian granites at some locations, as is typical for the Hesperic Massif (Ferreira, 1978). The soils were mapped, at a scale of 1: 1.000.000, as predominantly Humic Cambisols (Cardoso et al., 1971, 1973). However, field descriptions of soil profiles at the various study sites suggested a prevalence of Leptosols (WRB, 2006) (see Machado et al., 2015; Martins et al., 2013). Soil texture of the A-horizon was also determined in the field, and was slightly coarser for the soils on granite (sandy loam) than for the soils on schist (sandy clay loam). The topsoil was very rich in organic matter, amounting to 20-30 % at 0-2 cm depth (Machado et al., 2015) and 8-11 % at 0-5 cm depth (Prats et al., 2014).

Within the burnt area, a total of six study sites were selected to study post-fire runoff and erosion (Figure 1; Table 1). They consisted of four eucalypt plantations on schist (sites B, D, E, S), one eucalypt plantation on granite (site A) and one pine plantation on schist (site C), basically following the incidence of these land cover-parent material combinations in the burnt area. In addition, a long-unburnt eucalypt plantation was selected in the immediate vicinity of the burnt area (site F). Furthermore, one of the catchments within the burnt area was selected to study the hydrological and erosion response at the catchment scale.

3. Materials and Methods

3.1. Experimental set-up and collection of runoff samples

Five of the six study sites within the burnt area - i.e. except site S - were divided in three adjacent strips running from the base to the top of the slope (section) (Machado et al., 2015; Martins et al., 2013). In one of these strips, either three bounded micro-plots (0.25-0.30 m^2) were installed at the slope's base (sites A, B and C, for being located within the catchments and therefore to minimize disturbance) or two pairs of such micro-plots were installed at the base and halfway the slope (site D and E). In another strip, one (un-)bounded slope-scale plot with a width of approximately 2 m and contributing areas exceeding 50 m^2, depending on slope length, was installed. Each slope-scale plot, however, comprised four outlet that were connected to different runoff-collecting tanks. Site S involved a more elaborate experimental design, as it had been selected to assess the effectiveness of two treatments to reduce soil erosion, i.e. mulching with forest residues and application of a dry granular anionic polyacrylamide (PAM; Prats et al., 2014, 2015). Polyacrylamides have been found to markedly reduce soil losses from agricultural fields and road embankments (Ben-Hur, 2006). Four triplets of the above-mentioned micro-plots were installed from the base to the top of slope S to assess the effectiveness of both treatments. Furthermore, two bounded slope-scale runoff plots of 4 m wide by 20-25 m long were installed to assess the effectiveness of mulching with forest residues. The unburnt site, on the other hand, involved a simpler experimental design as it was relatively narrow and could only divided in two strips. Therefore, it was only instrumented with a unbounded slope-scale plot as described above.

The runoff from the micro-plot and the individual outlets of the slope-scale plots was collected in tanks of 30 and 80500 L, respectively. Runoff volume in the tanks was measured and runoff samples were collected in 1.5 L bottles, following intensive stirring of the water in the tanks. This was done at 1- to 2-weekly intervals, depending on rainfall, starting at the end of August 2010 when the site instrumentation had been completed.

The outlet of the experimental catchment was instrumented with a hydrological station comprising two flumes, two water level recorders and an automatic sampler that was triggered by a data logger based on the readings of the two water level recorders.

3.2. Laboratory analysis of runoff samples

For this study, a total of 1139 runoff samples were analyzed, of which 158 concerned streamflow, and 565 and 416 overland flow at the slope and micro-plot scale, respectively. The distribution of the latter samples over the different sites is given in Table 1. The samples were collected during the first year after the wildfire, as further detailed in Table 1, except for 36 micro-plot samples that were collected at the S site between the end of October 2011 and early January 2011.

The sediment concentration of these samples was determined in the laboratory using the classic filtration method (APHA, 1998), employing filter paper with a pore diameter of 12-

14 μm and drying the filters in an oven at 105 ºC for 24 hours. Furthermore, the organic matter content of the filtered sediments was determined using the loss-on-ignition method, placing the filters in a muffle for 4 h at 550 °C.

For each of the runoff samples, the normalized loss of the transmitted light - i.e. the ratio of the loss of light transmitted through a runoff sample and transmitted through a reference sample of bi-distilled water - was determined using the plastic optical fiber (POF) turbidity sensor presented by Bilro et al. (2010) but with a slightly modified design of the sensor head. To this end, the sensor head was first placed within a plastic recipient with bi-distilled water to measure the reference signal and then within a second recipient with the runoff sample to measure the light loss due to the sediments that were being kept in suspension by means of a magnetic agitator. The measurements were carried out during a period of 1 minute, during which the POF sensor performed 120 readings. Following visual inspection for and possible elimination of anomalous readings, the average values of both sets of readings were then used to compute the normalized transmitted light loss.

3.3. Data analysis

The sediment concentrations of the runoff samples from the micro-plots and the slope-scale plots were tested for significant differences, at $\alpha = 0.05$, between the treatments at site S as well as between the sites using non-parametric tests. The Kruskal-Wallis test was employed in case of multiple groups and, in case of significant results, followed by multiple pairwise comparisons using post-hoc probabilities corrected for the number of comparisons. The Mann-Whitney U-test was employed in the case of two groups. All statistical tests were carried out using STATISTICA 9.0 for Windows (© Stat Soft. Inc.).

The relationships of sediment concentrations with normalized light loss were determined using the Origin software (©OriginLab). In a first phase, a range of possible functions (first to fourth order polynomials, exponential, Napierian logarithmic and power) were fitted to the entire sets of micro-plot samples, slope-scale samples and catchment-scale samples. Overall, the third and fourth order polynomials and the exponential functions provided the best fits, with identical adjusted R^2's (0.73, 0.87 and 0.85, respectively). Nonetheless, the power function was preferred for the ensuing results, since the differences in R^2's were considered too small (≤0.02) to justify the additional one or two unknowns of the other functions.

4. Results and discussion

4.1. Micro-plot scale

4.1.1. Within-site differences related to erosion mitigation treatments

In line with the findings of Prats et al. (2014) regarding specific soil losses, the sample sets of the three treatments differed significantly in sediment concentrations (Table 2). The median sediment concentration of the untreated samples was 35 % lower than that of the PAM samples but almost three times higher than that of the mulching samples. The median organic matter contents of all three sample sets were high (52-67 %), suggesting that charred material was a major component of the sediments exported under all three treatments. These median values closely matched the average values in Prats et al. (2014), attesting to the representativeness of the sample sets included in this study. Furthermore, they agreed well with the figures in Malvar et al. (2011, 2013) for sediments eroded during the first two years following fire.

All three sample sets revealed a relationship of increasing normalized light loss with increasing sediment concentration (Figure 2), as was expected based on the findings with an earlier proto-type of the turbidity sensor (Bilro et al., 2010, 2011). The power function provided reasonably good fits of these relationships in all three instances, with adjusted R^2's ranging from 0.64 in the case of the untreated samples to 0.72 in the case of the PAM samples (Table 2). Bilro et al. (2011) found clearly better fits ($R^2 > 0.95$) for clay as well as ash particles but the authors used dilution series of artificial samples rather than runoff samples collected in the field.

The curves fitted to the untreated and the PAM samples were very similar, at least within the range of measured sediment concentrations (i.e. < 8.5 gL-1). Possibly, the somewhat divergent curve of the mulching samples was due to smaller range of measured sediment concentrations (< 2.5 gL-1), also because the relationships between sediment concentration and normalized light loss seemed to reveal more spread at higher concentrations.

4.1.2. Between-site differences related to land cover and parent material

Conspicuous and, in various instances, significant differences existed between the study sites in the sediment concentration of the micro-plot runoff samples (Table 2). Median sediment concentrations appeared to be influenced by both parent material and forest type, as median values were significantly lower for the pine plantation on schist (0.08 gL-1) and for the eucalypt plantation on granite (0.13 gL-1) than for the eucalypt plantations on schist (≥ 0.21 gL-1). Significant differences, however, also existed among the eucalypt plantations on schist, with the median sediment concentration of the D site (0.21 gL-1) being 3.5 times lower than that of the E site (0.73 gL-1). Between-site differences did not seem to be related to fire severity, at least as suggested by the field indicators used in this study (see section 2). The difference in median sediment concentration between the pine plantation on schist and the eucalypt plantation on granite agreed well with the difference in the sites' median specific sediment losses reported by Martins et al. (2013: 0.08 vs. 0.16 g m^{-2} mm^{-1} of runoff), once again testifying to the representativeness of the sample sets included in this study.

The untreated sample sets from all six study sites showed the expected increases in normalized light loss with increasing sediment concentrations. Furthermore, these increases agreed well with power functions, with the adjusted R^2's of the fitted curves ranging from 0.64 to 0.81 (Figure 3; Table 2). The fits were somewhat worse for sites D and S than for the remaining four sites (adjusted R^2's: 0.64-0.67 vs. 0.76-0.81) but this difference was apparently unrelated to parent material, forest type, sediment concentrations or their organic matter contents. However, the shape of the fitted curves did seem related to sediment concentrations. The curves were steeper for sites A, C and D than for sites B, E and S, and the former three sites had clearly lower median, third quartile and maximum sediment concentrations than the latter three sites (e.g., in the case of maximum concentrations, 0.91-1.48 vs. 3.89-7.48 gL-1). This contrast could be due to differences in the size of the exported sediment particles, since the sensor's light attenuation was shown to decrease with increasing particle size (Bilro et al., 2011) and since the lower sediment concentrations at sites A, C and D could be explained by overland flow with a lower transport capacity, preferentially exporting smaller particles. Nonetheless, the contrast could also be an artifact from the lower ranges of sediment concentrations measured at sites A, C and D, as these ranges only covered the initial, steeper parts of the fitted curves.

4.2. Slope scale

4.2.1. Within-site differences related to erosion mitigation treatment

Like the micro-plot samples, the slope-scale samples revealed clear and significant differences in sediment concentration between the untreated and mulching samples (Table 3). The median sediment concentration of the untreated samples was more than three times higher than that of the mulching samples (0.63 vs. 0.19 gL-1). These differences agreed well with the stronger runoff response of the untreated than mulched plot during the first year after fire (Prats et al., 2015: 58 vs. 30 mm).

The slope-scale samples tended to have higher median, third quartile and maximum sediment concentrations than the micro-plot samples of the same treatment (Table 3). The only exception was the maximum sediment concentration of the mulched samples, being 20 % lower in the case of the slope-scale samples than of the micro-plot samples (1.74 vs. 2.19 gL-1). This tendency in sediment concentrations was opposed to that in overland flow, as Prats et al. (2015) reported roughly 15 times less overland flow at the slope than micro-plot scale (409-956 vs. 30-58).

The fit of the power function was substantially better for the slope-scale samples than for the micro-plot samples in the case of the untreated plot but basically the same in the case of the mulched plot (Table 3; adjusted R^2's: 0.85 vs 0.64 and 0.71 vs. 0.69, respectively). In both cases, light loss with increasing sediment concentration was larger for the slope-scale samples than for the micro-plot samples (Figure 4). Only in the case of the mulching samples, however, this was due to a clearly higher attenuation coefficient (0.75 vs. 0.66) and, as referred earlier, could be explained by a greater prevalence of smaller particles in the slope-scale than micro-plot samples (see Bilro et al., 2011), reflecting a reduced transport capacity of the overland flow. This explanation could also account for the lower median organic matter concentration of the slope-scale samples, with the larger charred particles being beyond the runoff's detachment/transport capacity.

4.2.2. Between-site differences related to fire, land cover and parent material

The slope-scale samples tended to have higher median, third quartile and maximum sediment concentrations than the micro-plot samples, as was also noted in the previous section. At the same time, however, they revealed similar contrasts between the six burnt study sites, except in the case of the eucalypt plantation on granite (Table 3). The median sediment concentration was significantly lower for the pine plantation (0.11 gL-1) than for the burnt eucalypt plantations (on schist and granite; ≥ 0.29 gL-1). The median sediment concentration for the eucalypt plantation on granite lied within the range of values for the other eucalypt plantations, unlike was the case for the micro-plot samples. This reflected a comparatively large increase in median sediment concentration from the micro-plot to slope scale. This was in line with the findings of Machado et al. (2015), who reported a marked increase in sediment losses with spatial scale for the eucalypt plantation on granite (from 50 to 140 g m^{-2}) as opposed to clear decreases for the pine plantation as well as for the eucalypt plantation on schist at the B site (from 85 and 200 to 3.5 and 6.1 g m^{-2}, respectively).

The sediment concentrations for the unburnt eucalypt plantation were significantly lower than those for the burnt eucalypt plantations. This agreed with the slope-scale sediment losses reported by Machado et al. (2015), being clearly lower for the unburnt than burnt eucalypt site on schist (1.2 vs. 3.5 g m-2).

Better fits of the power function were obtained for the slope-scale samples than for the micro-plot samples in the case of five of the six burnt study sites, the pine site being the exception (Table 3). The pine plantation also stood out for its low adjusted R^2 (0.72) as compared to the other burnt plantations (0.83-0.89). The R^2 was similarly low for the mulching samples (0.71) and even considerably lower for the samples from the unburnt eucalypt stand (0.52), suggesting an association between poor fits and reduced sediment concentrations, unlike was the case for the micro-plot samples.

The best-fitting curves for the slope-scale samples revealed a greater similarity between the six burnt plantations than those for the micro-plot samples (Figure 4). Among the burnt plantations, only the D site stood out but mainly because of a comparatively low base constant rather than a different attenuation coefficient. For the same reason, the curve for the long-unburnt plantation stood out even more from those of the burnt plantations. The discrepancy of these two curves could well be an artifact from the comparatively low sediment concentrations measured at the D and F sites, also because possible differences in particle size due to reduced transport capacity would point to steeper curves as was the case of the curves fitted to the micro-plot samples of sites A, C and D (see section 4.1.2). Unlike in the case of these latter three sites, the curves fitted to the slope-scale samples of sites B and E agreed particularly well with those fitted to the sites' micro-plot samples. This suggested that wider ranges of measured sediment concentrations provided a more reliable basis for a consistent relation between turbidity and sediment concentrations over spatial scales as well as across study sites.

4.3. Catchment scale

The sediment concentrations of the streamflow samples were more similar to those of slope-scale samples from the B site than from the A and C sites (Table 4)., This fitted in well with the fact that the B site represented the dominant land cover-parent material combination within the catchment (Table 4). Nonetheless, the maximum value of the streamflow samples was well below the maximum values for all three slopes (4.55 vs. ≥6.59 gL-1). Also the median organic matter concentration of the streamflow samples was comparatively low (22 vs ≥38 %). Even so, it was substantially higher than the organic matter content of the sediments deposited as bed load within the flume at the catchment outlet (Keizer et al., 2015: 5 %).

The power function provided a good fit to the relationship of increasing normalized light loss with increasing sediment concentration as revealed by the streamflow samples, with an adjusted R^2 of 0.85 (Table 4). The fitted curve, however, differed considerably from the curves fitted to slope-scale samples of the three slopes located within the catchment. The stronger attenuation coefficient for the streamflow samples (0.71 vs. 0.57-0.60) could be due to a prevalence of smaller particles in suspension, especially because of the deposition of sediments in the flume at the catchment outlet as well as in two upstream retention ponds (see Keizer et al., 2015).

5. Conclusions

The principal conclusions of this study into the performance of a novel plastic optical fiber (POF) turbidity sensor for measuring soil erosion following wildfire were the following:

(i) the observed sediment concentrations were within the measurement range of the POF sensor, attesting to the suitability of the sensor to be employed during the initial phases of the so-called window-of-disturbance when erosion losses tend to be highest and when exported sediments tend to contain highest contents of - charred - organic matter;

(ii) the relationships of sediment concentration with normalized light loss varied markedly with spatial scale and, in particular, between micro-plot and slope-scale samples, on the one hand, and, on the other, catchment-scale samples, suggesting that scale-specific calibration curves are required to guarantee optimal sensor performance;

(iii) the slope-scale relationships of sediment concentration with normalized light loss varied clearly less between study sites than the micro-plot scale relationships, indicating that the need for site-specific calibration curves is greater when sediment concentrations and, thus, erosion rates are comparatively low;

(iv) the previous conclusion was also suggested by the comparison of the sediment concentrations with and without an effective erosion mitigation treatment;

(v) the POF sensor would allow to speed up considerably the processing of the runoff samples in the laboratory (and, perhaps, even in the field) and, at the same time, would permit an efficient, stratified-sampling approach towards the construction of a scale- and/or site-specific calibration curves.

Given the very satisfactory performance of the sensor in this study, further work will include redesigning the sensor and, in particular, its head to make it more robust and more easy to handle, testing the new sensor for continuous monitoring of stream flow turbidity under field conditions, and optimizing data processing algorithms,

Acknowledgements

The present study was carried out in the framework of the projects TRANFIBRA (project nr 23148) and FIRECNUTS (PTDC/AGRCFL/104559/2008), funded by FEDER, through the Agência de Inovação S.A., in the framework of the QREN SI I&DT program and funded by FCT/MCTES (PIDDAC), with co-funding by FEDER through COMPETE (Programa Operacional Factores de Competitividade; POFC), respectively. Additional financial support was provided by the EU-FP7 project RECARE (contract number grant agreement 603498). We further gratefully acknowledge the help of various colleagues of the earth surface processes team with field data and sample collection and/or with laboratory analysis of the sediment samples. Finally, we would like to acknowledge the comments and suggestions by the

handling editor as well as by the three anonymous reviewers, which helped to improve this manuscript considerably.

References

APHA - American Public Health Association. Total suspended solids dried at 105 degrees Celsius method 2540D. In: Standard Methods for the Examination of Water and Waste Water, 20th ed., Washington, DC, USA, 1998.

Ben-Hur, M. Using synthetic polymers as soil conditioners to control runoff and soil loss in arid regions – a review. AUST J SOIL RES 44, 191-204, 2006.

Bilro, L., Prats, S.A., Pinto, J.L., Keizer, J.J., Nogueira, N. Design and performance assessment of a POF based sensor for measuring water turbidity. MEAS SCI TECHNOL 21, 10, 107001, 2010.

Bilro, L., Prats, S., Pinto, J.L., Keizer, J.J., Nogueira, R. N. Turbidity sensor for determination of concentration, ash presence and particle diameter of sediment suspensions. Proceedings of Spie, Vol 7753, doi: 10.1117/12.885112, 2011.

Campbell, C., Laycak, D., Hoppes, W., Tran, N.T., Shib, F. High concentration suspended sediment measurements using a continuous fiber optic in-stream transmissometer. J HYDROL 311(1–4), 244–253, 2005.

Cardoso, J.C., Bessa, M.T., Marado, M.B. Carta dos solos de Portugal (1:1,000,000). Serviço de Reconhecimento e de Ordenamento Agrário, Secretaria de Estado da Agricultura, Lisbon, Portugal, 1971.

Cardoso, J.C., Bessa, M.T., Marado, M.B.Carta dos solos de Portugal (1:1,000,000). Agronomia Lusitana 33, 461–602, 1973.

Cerdà, A. Changes in overland flow and infiltration after a rangeland fire in a Mediterranean shrubland. HYDROL PROCESS 12, 1031-1042, 1998.

Downing, J. Twenty-five years with OBS sensors: The good, the bad, and the ugly. CONT SHELF RES 26, 2299–2318, 2006

DRA-Centro - Direcção Regional do Ambiente do Centro. Plano de bacia hidrográfica do Rio Vouga, 1ª fase, Análise e diagnóstico da situação de referência, Análise biofísica, Anexos. Lisboa, Portugal, 1998.

DUDF - Direcção de Unidade de Defesa da Floresta. Relatório Anual de Áreas Ardidas e Ocorrências 2010. Autoridade Florestal Nacional, Lisboa, 2011.

Fernández, C., Veja, J.A., Fontúrbel, M.T., Pérez-Gorostiaga, P., Jiménez, E., Madrigal, J. Effects of wildfire, salvage logging and slash treatments on soil degradation. LAND DEGRAD DEV 18, 591–607, 2007.

Ferreira, A. de Brum. Planaltos e montanhas do norte da Beira – estudo de geomorfologia. Centro de Estudos Geográficos, Lisbon, Portugal, 1978.

Inbar, M., Tamir, M., Wittenberg, L. Runoff and erosion processes after a forest fire in Mount Carmel, a Mediterranean area. GEOMORPHOLOGY 24, 17–33, 1998.

Keeley, J.E. Fire intensity, fire severity and burn severity: A brief review and suggested usage. INT J WILDLAND FIRE 18, 1, 116-126, 2009.

Keizer, J.J., Martins, M.A.S, Prats, S.A., Faria, S.R., González-Pelayo, O., Machado, A.I., Rial-Rivas, M.E., Santos, L.F., Serpa, D., Varela, M.E.T. Within-in flume sediment deposition in a forested catchment following wildfire and post-fire bench terracing, north-central Portugal. Cuadernos de Investigación Geográfica 41(1), 149-164, 2015.

Lavabre, J., Martin, C. Impact d'un incendie de forêt sur l'hydrologie et l'érosion hydrique d'un petit bassin versant méditerranéan. Human Impact on Erosion and Sedimentation (Proceedings of Rabat Symposium S6, April 1997): IAHS Publication 245, pp. 39–47, 1997.

Lane, P.N.J., Sheridan, G.J., Noske, P.J. Changes in sediment loads and discharge from small mountain catchments following wildfire in south eastern Australia. J HYDROL 331, 495– 510, 2006.

Machado, A.I., Serpa, D.R., Ferreira, R.S.V., Rodríguez-Blanco, M.L., Pinto, R., Nunes, M.I., Cerqueira, M.M., Keizer, J.J. Cation export by overland flow in a recently burnt forest area in north-central Portugal. SCI TOTAL ENVIRON 524–525, 201–212, 2015.

Malvar, M.C., Prats, S.A., Nunes, J.P., Keizer, J.J. Post-fire overland flow generation and inter-rill erosion under simulated rainfall in two eucalypt stands in north-central Portugal. ENVIRON RES 111, 222-236, 2011.

Malvar, M.C., Martins, M.A., Nunes, J.P., Robichaud, P.R., Keizer, J.J. Assessing the role of pre-fire ground preparation operations and soil water repellency in post-fire runoff and inter-rill erosion by repeated rainfall simulation experiments in Portuguese eucalypt plantations. CATENA 108, 69-83, 2013.

Martins, M.A.S., Machado, A. I., Serpa, D., Prats, S.A., Faria, S.R., Varela, M.E.T., Gonzalez-Pelayo, O., Keizer, J.J. Runoff and inter-rill erosion in a Maritime Pine and a eucalypt plantation following wildfire and terracing in north-central Portugal. Journal of Hydrology and Hydromechanics 61, 4, 261-269, 2013.

Mayor, A.G., Bautista, S., Llovet, J., Bellot, J. Post-fire hydrological and erosional responses of a Mediterranean landscape: seven years of catchment-scale dynamics. CATENA 71, 68–75, 2007.

Moody, J.A., Shakesby, R.A., Robichaud, P.R., Cannon, S.H., Martin, D.A. Current research issues related to post-wildfire runoff and erosion processes. EARTH-SCI REV 122, 10–37, 2013.

Omar, A.F.B., MatJafri, M.Z.B. Turbidimeter design and analysis: a review on optical fiber sensors for the measurement of water turbidity. Sensing 9(10), 8311–8335, 2009.

Postolache, O.A., Silva Girao, P.M.B., Dias Pereira, J.M., Ramos, H.M., 2007. Multibeam optical system and neural processing for turbidity measurement. IEEE Sensing Journal 7, 677–684, 2007.

Prats, S.A., Martins, M.A.S., Malvar, M.C., Ben-Hur, M., Keizer, J.J. Polyacrylamide application versus forest residue mulching for reducing post-fire runoff and soil erosion. SCI TOTAL ENVIRON 468-469, 464-474, 2014.

Prats, S.A., Wagenbrenner, J.W., Martins, M.A.S., Malvar, M.C., Keizer, J.J. Hydrological implications of post-fire mulching across two spatial scales. LAND DEGRAD DEV, 2015 (in press; doi 10.1002/ldr.2422).

Robichaud, P.R., Elliot, W.J., Pierson, F.B., Hall, D.E., Moffet, C.A. Predicting postfire erosion and mitigation effectiveness with a web-based probabilistic erosion model. CATENA 71, 229–24, 2007.

Ruhl, C.A., Schoellhamer, D.H., Stumpf, R.P., Lindsay, C.L. Combined use of remote sensing and continuous monitoring to analyse the variability of suspended-sediment concentrations in San Francisco Bay, California. ESTUAR COAST SHELF S 53(6), 801–812, 2001.

Shakesby, R. Post-wildfire soil erosion in the Mediterranean: review and future 730 research directions. EARTH-SCI REV 105, 71-100, 2011.

Shakesby, R.A., Doerr, S.H. Wildfire as a hydrological and geomorphological agent. EARTH-SCI REV 74, 269–307, 2006.

Thomas, A.D., Walsh, R.P.D., Shakesby, R.A. Nutrient losses in eroded sediment after fire in eucalyptus and pine forests in the wet Mediterranean environment of northern Portugal. CATENA 36, 283–302, 1999.

WRB - World reference base for soil resources. World Soil Resources Reports, 103. FAO, Rome, 2006.

Yeo, T.L., Sun, T., Grattan, K.T.V. Fibre-optic sensor technologies for humidity and moisture measurement. SENSOR ACTUATOR A 144, 280–295, 2008.

Ziemann, O., Krauser, J., Zamzow, P.E., Daum, W. POF Handbook – Optical Short Range Transmission Systems, 2nd edition, Springer-Verlag, Berlin Heidelberg, 2008.

Table 1. General information about the seven study sites as well as the numbers of runoff samples from micro-plots and slope-scale plots analyzed from each site and the start and end dates of collecting these samples (in ddmmyy)

Site code	Location		Wild-fire	Forest type	Parent material	Treat-ment	Micro-plots			Slope-scale plots		
	Lat	Lon					N	start	end	N	start	end
S	40°44'05"N	8°21'18"N	burnt	euc.	schist	none	112	260810	040112	89	260810	240811
						PAM	78	260810	070911	-	260810	-
						mulching	57	260810	070911	85	260810	070911
B	40°43'59"N	8°20'58"N	burnt	euc.	schist	none	33	260810	230211	45	260810	230211
D	40°43'29"N	8°20'57"N	burnt	euc.	schist	none	47	260810	290411	90	260810	240811
E	40°44'04"N	8°21'16"N	burnt	euc.	schist	none	42	260810	180511	70	260810	240811
A	40°43'56"N	8°21'3"N	burnt	euc.	granite	none	19	260810	230211	73	260810	230210
C	40°43'54"N	8°20'47"N	burnt	pine	schist	none	28	260810	230211	57	260810	180511
F	40°44'16"N	8°20'45"N	unburnt	euc.	schist	none	-	-	-	56	260810	010611

Table 2. Sediment concentrations and corresponding organic matter (OM) contents of the micro-plot scale overland flow samples at the six study sites, and best-fitting power functions between sediment concentration (x; in gL-1) with normalized light loss (y).   Euc. = eucalypt; med = median; iqr = inter-quartile range; 3^{rd} q = third quartile; max = maximum; sign = statistically significant differences, at α = 0.05, are indicated by different roman numbers in the case of the treatments tested at the S site and by different letters in the case of the other sites.

Site code	Forest type	Parent material	Treat-ment	N	Sediment concentration gL-1					OM content %		Best-fitting power function	Ad-justed R2
					med	iqr	3rd q	max	sign	med	iqr		
S	euc.	schist	none	112	0.41	0.53	0.72	7.48	ii	61	24	y = 0.1735x^0.5983	0.64
			PAM	78	0.64	1.07	1.37	8.19	iii	52	22	y = 0.1962x^0.5247	0.72
			mulching	57	0.14	0.20	0.27	2.19	i	67	21	y = 0.1268x^0.6577	0.69
B	euc.	schist	none	33	0.38	0.66	0.85	3.89	cd	54	12	y = 0.2965x^0.4938	0.77
D	euc.	schist	none	47	0.21	0.16	0.27	1.06	bc	55	14	y = 0.2054x^0.8090	0.67
E	euc.	schist	none	42	0.73	1.76	2.00	6.06	d	64	29	y = 0.2510x^0.5372	0.76
A	euc.	granite	none	19	0.13	0.16	0.22	0.91	ab	58	18	y = 0.2971x^0.7912	0.81
C	pine	schist	none	28	0.08	0.12	0.15	1.48	a	54	12	y = 0.2808x^0.6794	0.76

Table 3. Sediment concentrations and corresponding organic matter (OM) contents of the slope- scale overland flow samples at the seven study sites, and best-fitting power functions between sediment concentration (x; in gL-1) with normalized light loss (y). Euc. = eucalypt; med = median; iqr = inter-quartile range; 3^{rd} q = third quartile; max = maximum; sign = statistically significant differences, at α = 0.05, are indicated by different roman numbers in the case of the treatments tested at the S site and by different letters in the case of the other sites.

Site code	Wild-fire	Forest type	Parent material	Treat-ment	N	Sediment concentration gL-1					OM content %		Best-fitting power function	Ad-justed R2
						med	iqr	3rd q	max	sign	med	iqr		
S	burnt	euc.	schist	none	89	0.63	1.07	1.35	8.99	ii	64	16	y = 0.2272x^0.6095	0.85
				mulching	85	0.19	0.41	0.51	1.74	i	47	23	y = 0.2163x^0.7510	0.71
B	burnt	euc.	schist	none	45	0.63	0.75	1.09	8.14	bcd	58	15	y = 0.2576x^0.5670	0.89
D	burnt	euc.	schist	none	90	0.29	0.84	1.00	5.86	bc	55	14	y = 0.1704x^0.6707	0.87
E	burnt	euc.	schist	none	70	1.21	2.26	2.86	8.62	cd	53	12	y = 0.2768x^0.5262	0.83
A	burnt	euc.	granite	none	73	0.69	1.12	1.39	6.59	bcd	38	12	y = 0.2356x^0.5944	0.86
C	burnt	pine	schist	none	57	0.11	0.32	0.35	6.60	a	53	19	y = 0.2281x^0.6020	0.72
F	unburnt	euc.	schist	none	56	0.05	0.14	0.15	0.74	a	78	22	y = 0.1314x^0.5832	0.52

Table 4. Sediment concentrations and corresponding organic matter (OM) contents of the streamflow samples at the catchment outlet, and best-fitting power function between sediment concentration (x; in gL-1) with normalized light loss (y). Med = median; iqr = inter-quartile range; 3rd q = third quartile; max = maximum.

N	Sediment concentration gL-1				OM content %		Best-fitting power function	Adjusted R2
	med	iqr	3rd q	max	med	iqr		
158	0.50	0.83	1.05	4.55	22	8	y = 0.2809x^0.7071	0.85

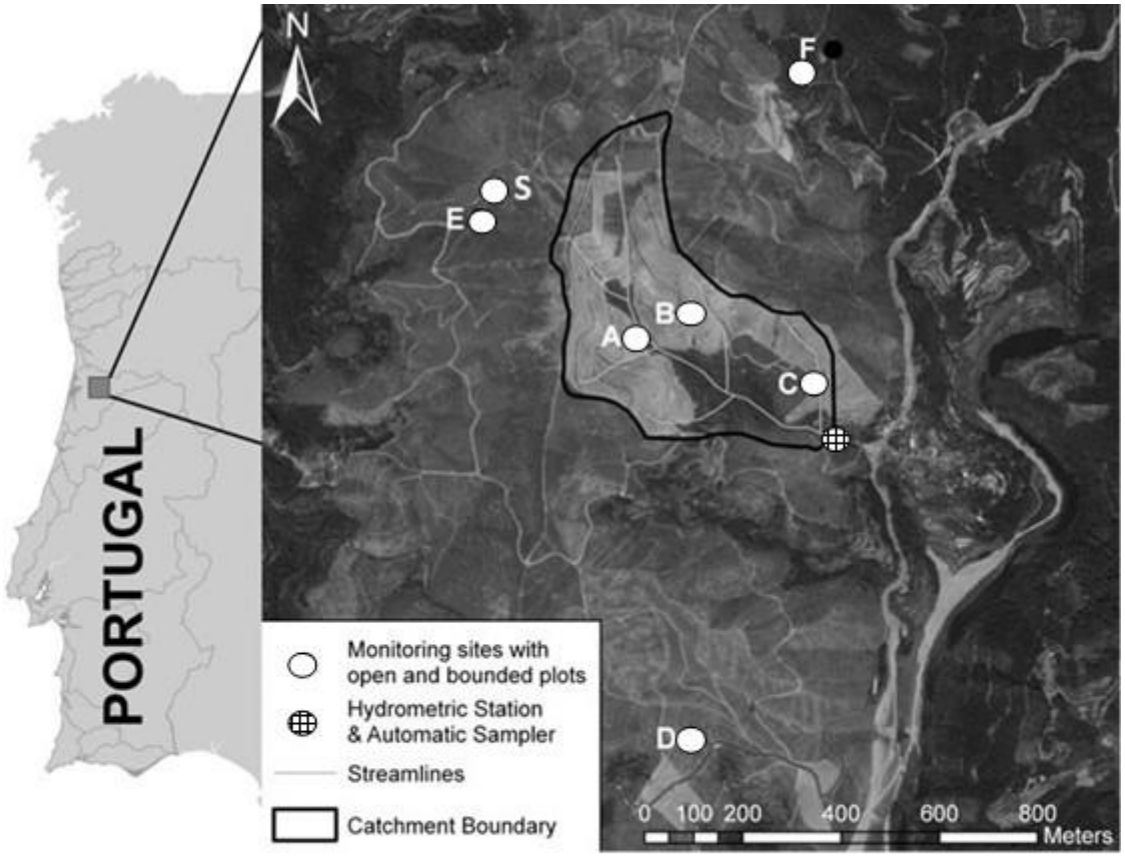

Figure 1. Location of the study area, the experimental catchment and the seven study sites (A = burnt eucalypt plantation on granite; B, D, E and S = burnt eucalypt plantations on schist; C = burnt pine plantation on schist; F = long-unburnt eucalypt plantation on schist).

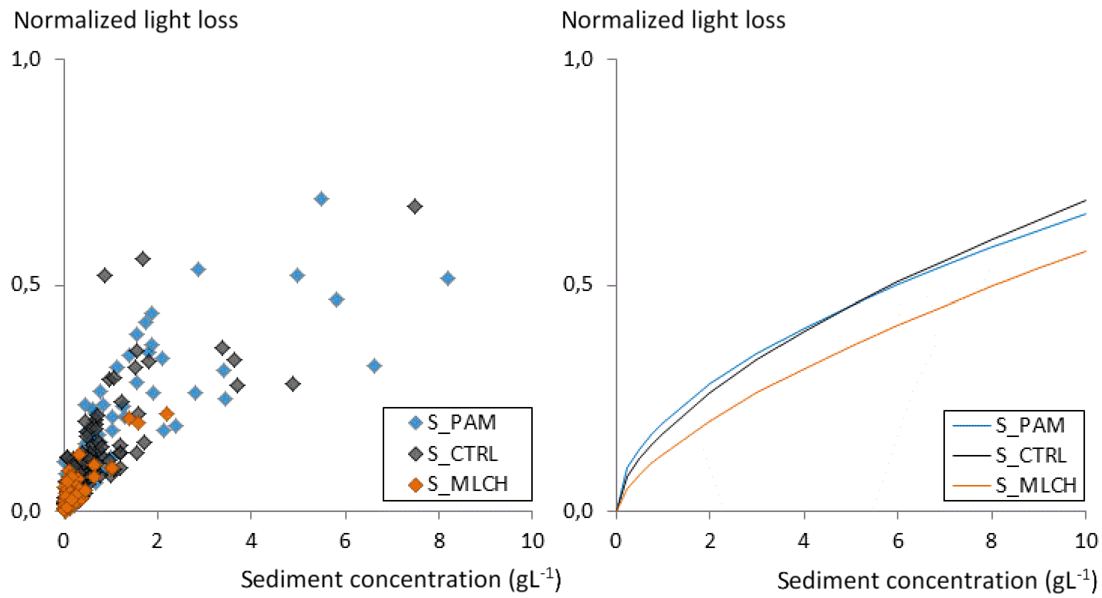

Figure 2. Relationships of sediment concentration with normalized light loss at the micro-plot scale for three treatments at study site S (left plot), and corresponding best-fitting power functions (right plot; see Table 2). S_PAM = polyacrylamide; S_CTRL = untreated; S_MLCH = mulching with forest residues.

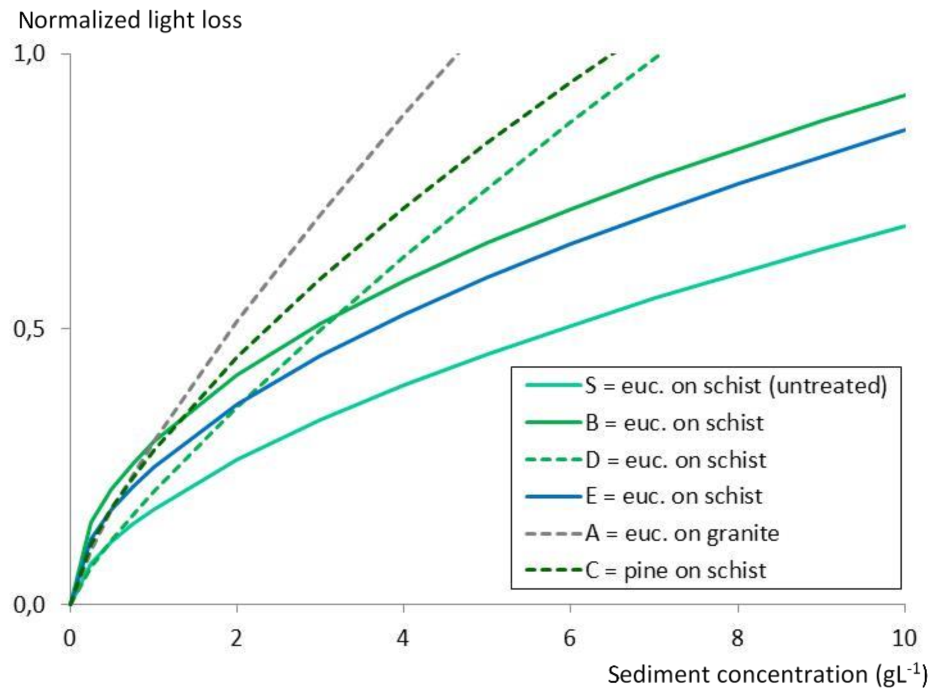

Figure 3. Best-fitting power functions of the relationships of post-fire sediment concentration with normalized light loss at the micro-plot scale for one pine plantation on schist and five eucalypt (euc.) plantations on schist or granite (see Table 2).

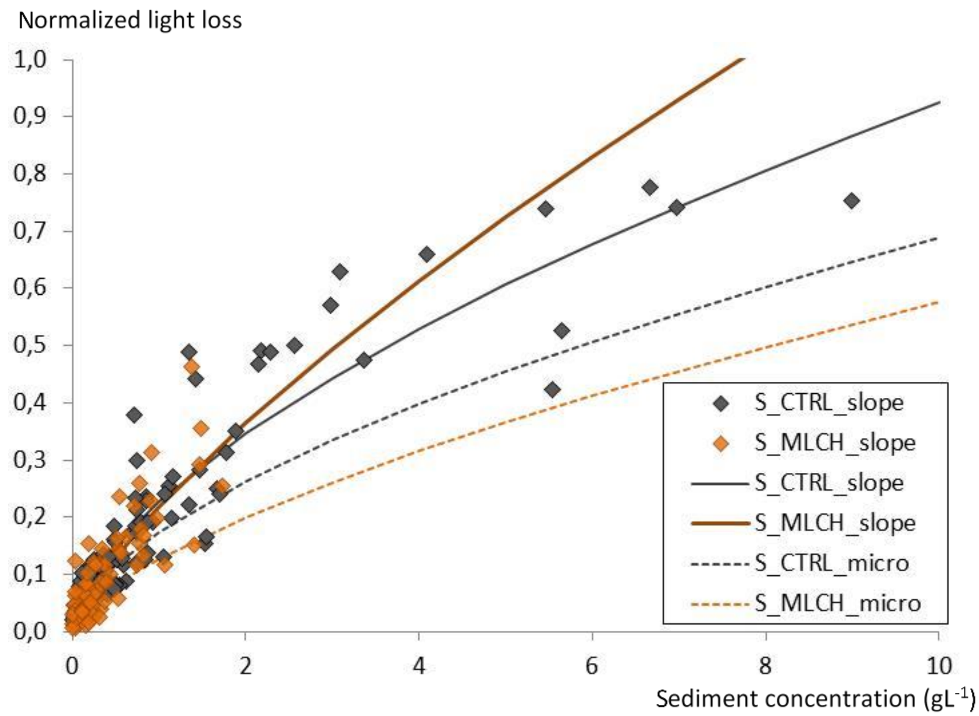

Figure 4. Relationships of post-fire sediment concentration with normalized light loss at the slope scale for two treatments at study site S (symbols), and best-fitting power functions at the slope as well as micro-plot scale (lines)(see Table 2 and 3). S_CTRL_slope/micro = untreated; S_MLCH_slope/micro = mulching with forest residues.

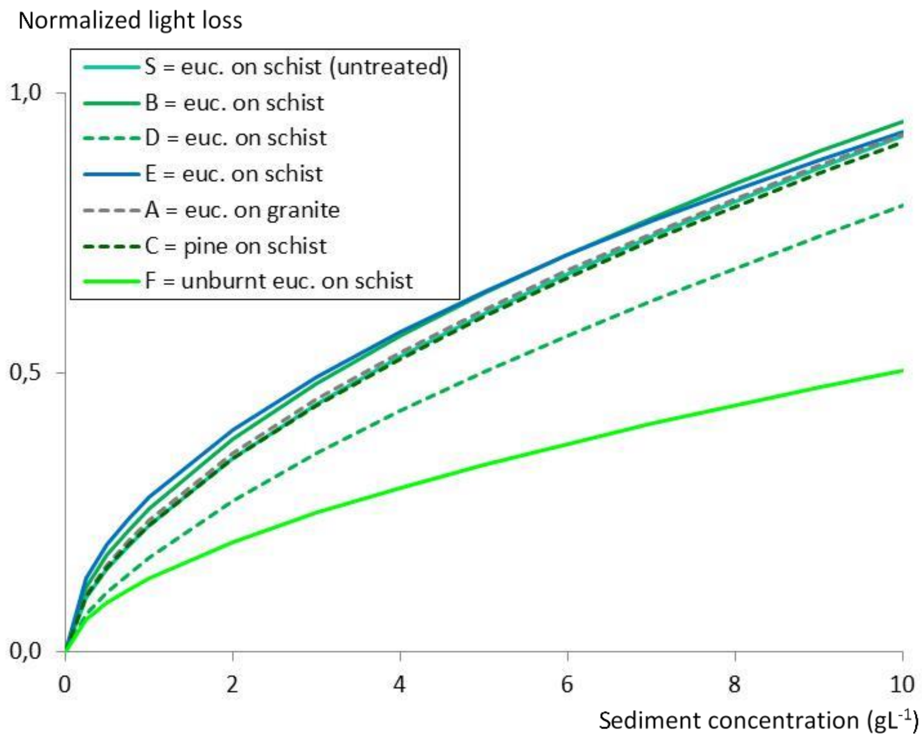

Figure 5. Best-fitting power functions of the relationships of sediment concentration with normalized light loss at the slope scale for one long-unburnt eucalypt (euc.) plantation on schist (F), five recently burnt eucalypt (euc.) plantations on schist or granite (A, B, D, E, S) and one recently burnt pine plantation on schist (C) (see Table 3).

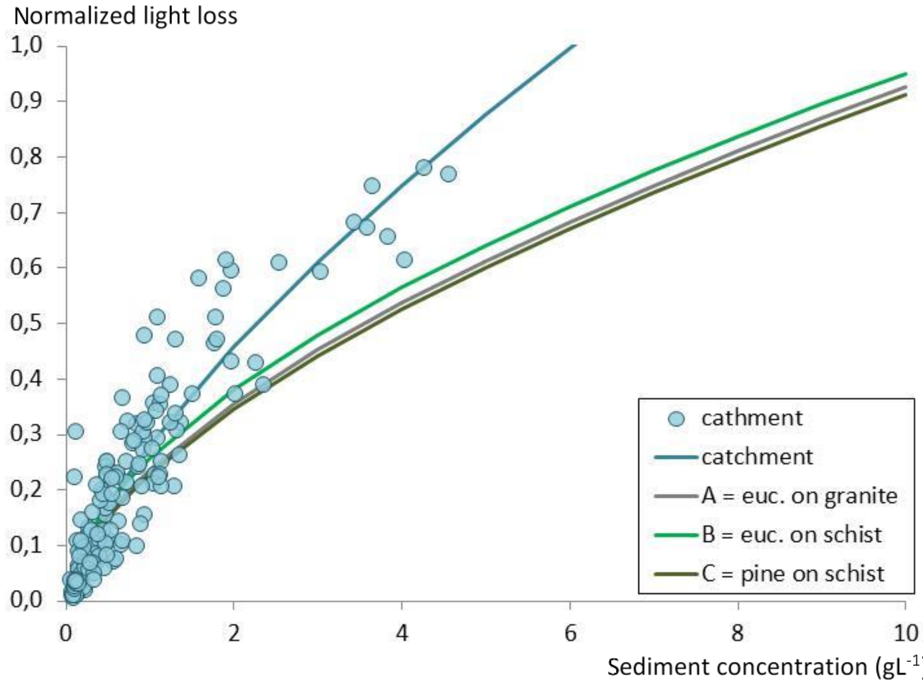

Figure 6. Relationships of sediment concentration with normalized light loss at the catchment scale(symbols) , and best-fitting power functions at the catchment as well as slope scale for the eucalypt (euc.) and pine plantations located within the catchment (see Table 3 and 4).